Fermilab FERMILAB-TM-2267-AD OCTOBER 2004

Beam dynamics in BTeV at top energy

T. Sen, J. Johnstone, M. Xiao
FNAL
PO Box 500
Batavia, IL 60510

Abstract

Beam dynamics of protons and anti-protons in a proposed BTeV lattice at 980 GeV is studied.

Contents

1 Introduction **2**

2 Single beam dynamics **2**
2.1 Tune shift with amplitude and dynamic aperture 2
2.2 Chromatic effects 5
2.3 Emittance growth due to intra-beam scattering 8

3 Beam-beam effects **11**
3.1 Dynamic Aperture 18
3.2 Diffusion and emittance growth due to the beam-beam interactions 18
3.3 Orbit changes and relative luminosities 19
3.4 Beam-beam effects on protons 20

4 Beam and Luminosity Lifetimes **22**

A Appendix: Error Harmonics **25**

1 Introduction

In this report we will consider beam dynamics in BTeV at top energy and low-beta. The major changes occur due to the new IR magnets at C0 where the beams will be brought to collision. The beams will be separated at B0 and D0. We consider the impact of the C0 IR magnets on the dynamic aperture of the beams. We also study the influence of the new helix on beam-beam interactions in BTeV. We will not consider collective effects in this report. Intensities of both beams in BTeV and at the end of Run II are expected to be nearly the same, so we do not expect new manifestations of collective effects in BTeV. Helix and optics changes for BTeV at injection, acceleration and squeeze are under study; we defer discussion of dynamics at these stages to a later date.

2 Single beam dynamics

The optics of the C0 insertion is taken to be that described in the C0 IR Technical Design Report [1]. The insertion is matched to the rest of the Tevatron at locations B38 and C17 and is designed to be transparent to the rest of the ring. The insertion increases the tunes of the Tevatron by one unit in each plane leaving the fractional tunes unchanged. Changes in the optics will affect the beam dynamics including the dynamic aperture, and emittance growth rates. In this section we will focus mainly on dynamic aperture calculations but also consider the emittance growth rates due to intra-beam scattering (IBS).

2.1 Tune shift with amplitude and dynamic aperture

When one beam is present, the nonlinear effects arise mainly from the magnetic nonlinearities. At low-beta, the beta functions in the low-beta triplets are the largest around the ring so the error fields in these quadrupoles strongly influence the dynamic aperture. The quadrupoles in the C0 insertion will have field quality similar to those built for the LHC. The table in Appendix A shows the expected field quality based on the prototypes built for the LHC.

Within the C0 IR quadrupoles, the design orbits go through the center of the vacuum chamber. Hence feed-down effects from the nonlinear fields in these quadrupoles will arise only in the presence of orbit errors. Orbit correctors local to the C0 insertion will therefore also be useful in minimizing the nonlinear effects.

The tune footprint due to the nonlinearities is a useful indicator of the resonances that could be important. Figure 1 compares the tune footprint for the Run II lattice with B0 and D0 at low-beta with the footprint for the BTeV lattice with only C0 at low-beta. For the Run II lattice, the errors were assumed to be the measured multipole errors. For errors in the C0 insertion, 5 random seeds were chosen from the distribution determined by the expected errors shown in Appendix A. The tune footprint in the bottom plot of this figure was obtained with one of the 5 seeds. Also shown in the bottom plot is the footprint in the BTeV lattice without nonlinear errors in the C0 low-beta quads. In all cases the tunes are calculated for particles with amplitudes up to 6σ in both planes. We observe that while the shape and orientation of the tune footprint is very different in the BTeV lattice compared to Run II, the tune spread is about the same $(8, 8) \times 10^{-4}$ for both lattices. The sources of the tune spread are the errors in the low-beta quadrupoles at B0 and D0 in Run II and, similarly, the errors in the low-beta quadrupoles at C0 for the BTeV lattice. For comparison,

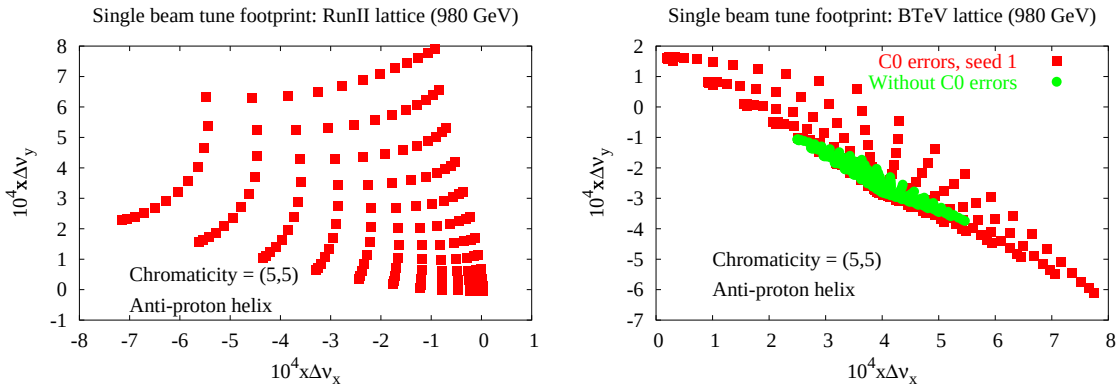

Figure 1: Tune footprint on the pbar helix at 980 GeV. Top: In the Run II lattice with B0 and D0 at low-beta. Bottom: Tune footprint with and without IR errors in C0 for the BTeV lattice. Only C0 is at low-beta in this case. Errors in the B0 and D0 insertions and the arcs are included in both cases. No beam-beam effects are included in either case.

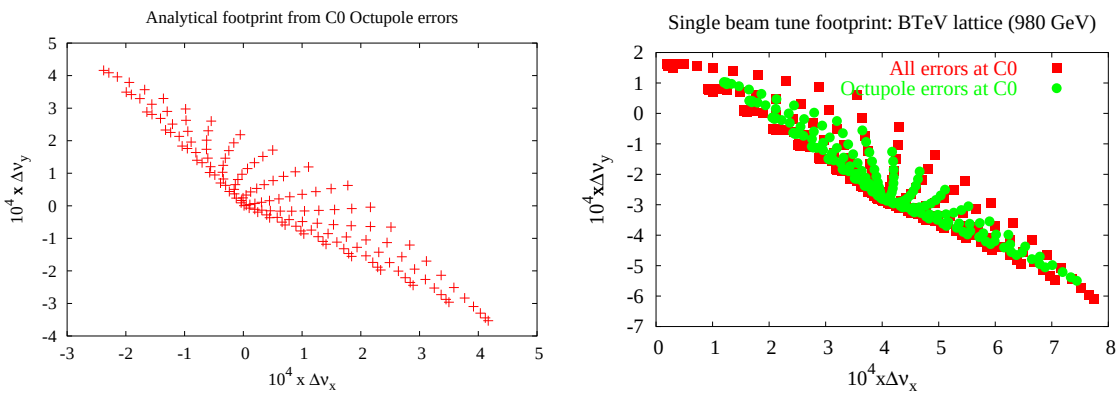

Figure 2: Left: Analytically calculated tune footprint due to octupole errors in the C0 insertion. Right: Tune footprint with all errors at C0 and only the octupole errors at C0. Errors in B0, D0 and the arcs are included in both cases. Note that the tune spread up to amplitudes of 6σ is (7,8)$\times 10^{-4}$.

the footprint without these errors in C0 are also shown in Figure 1, the spread is $(3,3)\times 10^{-4}$ - more than a factor of two smaller.

The tune footprint due to the octupoles can be calculated analytically. The tune dependence on amplitude due to octupoles is given by the following expressions

$$\begin{aligned}\Delta\nu_x(J_x,J_y) &= \frac{1}{16\pi}J_x\sum k_3(n)\beta_x^2(n) - \frac{1}{8\pi}J_y\sum k_3(n)\beta_x(n)\beta_y(n)\\ \Delta\nu_y(J_x,J_y) &= -\frac{1}{8\pi}J_x\sum k_3(n)\beta_x(n)\beta_y(n) + \frac{1}{16\pi}J_y\sum k_3(n)\beta_y^2(n)\end{aligned} \quad (1)$$

where (J_x, J_y) are the Courant-Snyder linear actions and the integrated octupole strength parameter is defined as

$$k_3 = K_3 L = \frac{1}{6}\frac{1}{(B\rho)}\frac{\partial^3 B_y}{\partial x^3}L$$

The tune shifts due to the octupole errors have been evaluated using these expressions.

The left plot in Figure 2 shows the analytically calculated tune footprint due to octupoles. We observe that the tune spread up to 6σ amplitudes is $(7,8)\times10^{-4}$, which agrees very closely with the tune spread found from simulations. The right plot in Figure 2 compares the footprint from only the octupoles with that from all the errors. We observe, as expected, that the single beam tune footprint is largely determined by the octupole errors. When multipole errors up to 12-pole are included, the tune footprint is virtually identical to the complete footprint. Thus the 14-pole to 20-pole errors do not have a significant influence on the tune footprint.

Thus the single beam tune footprint at low-beta in the BTeV lattice is of the same size as the similar footprint in the Run II lattice, is largely determined by the octupole errors in the low-beta quadrupoles and is well understood. As we will observe in the section on beam-beam effects, the tune footprint during collisions due to the head-on collision at C0 and the long-range interactions around the ring is more than an order of magnitude larger than the single beam tune footprint.

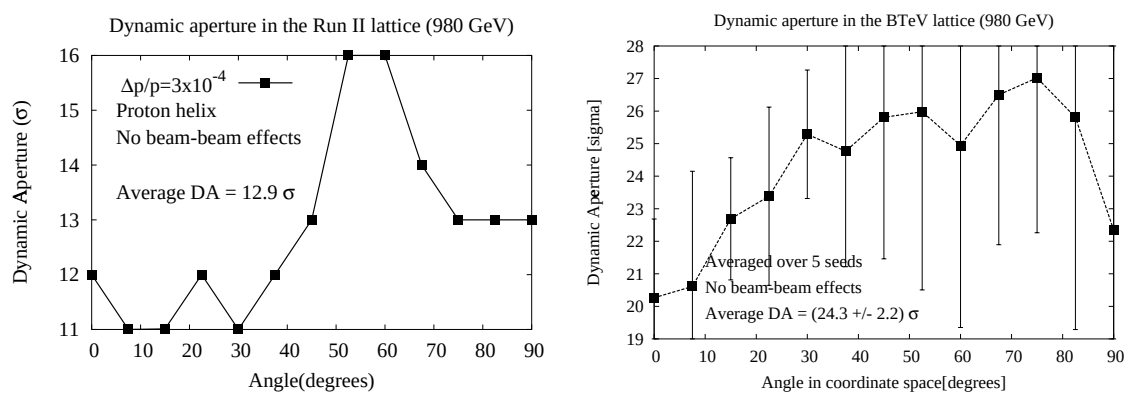

Figure 3: Single beam dynamic aperture on the proton helix at 980 GeV. Left: Run II lattice, Right: BTeV lattice.

Figure 3 shows the largest stable amplitude (in units of the rms beam size) as a function of the initial angle in coordinate space. Thus 0 degrees represents particles launched along the horizontal axis, and 90 degrees represents particles launched along the vertical axis. Tracking was done in all three degrees of freedom with synchrotron oscillations, amplitude of the momentum deviation $= 3 \times 10^{-4}$, chromaticity set to (5, 5) for both lattices. 200 particles were tracked for 100,000 turns. The errors for all magnets except for the C0 IR magnets were taken from a database maintained by N. Gelfand. The distribution of C0 IR errors were generated from the mean and rms values of the multipole components shown in Appendix A.

The dynamic aperture (DA) for the Run II lattice was calculated with the single set of errors while 5 random seeds for the C0 errors were used and the DA at each angle was averaged over the 5 seeds. The average single beam DA on the proton helix in the BTeV lattice is about 25σ, almost double the single beam DA in the Run II lattice. This confirms the expected result that the impact of the nonlinearities should decrease and the dynamic aperture increase in the BTeV lattice with only one insertion at low-beta.

While the real dynamic aperture in the Tevatron will be smaller than the theoretical values found here, the calculations done here indicate that the dynamic aperture for single beams will be larger in the BTeV lattice compared to the present Run II lattice. Thus the

	B0	D0	Run II total	BTeV
ξ_x	-16.7	-16.2	-32.9	-26.0
ξ_y	-15.6	-15.6	-31.2	-26.3

Table 1: Linear chromaticities of the low-beta triplet quadrupoles in Run II and in BTeV.

field quality specifications for the low-beta quadrupoles appear to be adequate.

2.2 Chromatic effects

The dynamic aperture in Section 2.1 was calculated with synchrotron motion included and linear chromaticity corrected to (5,5) units. However the machine chromaticity can and does adversely affect the beam lifetime in the Tevatron. Since these effects show up over a longer time scale than can be followed by tracking, it is important to check that the chromatic effects of the BTeV lattice are no worse than the present Run II lattice.

The linear chromaticity from individual quadrupoles can be calculated as

$$\xi \equiv -\frac{1}{4\pi}\sum_i (Q\beta)_i = -\frac{1}{4\pi}\sum_i (\int K(s)\beta(s)ds)_i \tag{2}$$

where the sum over i extends over the quadrupoles and the integration is done over the length of each quadrupole.

The linear chromaticity of the machine receives large contribution from the low-beta triplets due to their large gradients and large values of the beta functions in these quadrupoles. Table 1 shows the linear chromaticity contributions from each of low-beta triplets, assuming that each is at low-beta. The linear chromaticities from the BTeV triplets are individually larger than either of B0 and D0 but smaller than the sum of B0 and D0 combined. The smaller linear chromaticity should also reduce the required strengths of the chromaticity sextupoles.

In addition to the linear chromaticity, the low-beta triplets also generate a substantial chromatic beta-wave and as a consequence, large second order chromaticities [2]. The beta-wave can be split into a sum of non-chromatic terms and chromatic terms as

$$\frac{\Delta\beta(s)}{\beta(s)} = (\frac{\Delta\beta(s)}{\beta(s)})_0 + [(\frac{\Delta\beta(s)}{\beta(s)})_1\delta + (\frac{\Delta\beta(s)}{\beta(s)})_2\delta^2 + \ldots] \tag{3}$$

The first term on the right hand side contains the contributions of non-chromatic sources while the terms in the square brackets contains the chromatic sources of the beta-wave, expanded in a power series of the momentum deviation $\delta = \Delta p/p$. The linear chromatic beta-wave at a location s from a sequence of quadrupoles is

$$(\frac{\Delta\beta(s)}{\beta(s)})_1 = \frac{1}{2\sin 2\pi\nu_0}\sum_i (Q\beta)_i \cos[2|\psi(s) - \psi_i| - 2\pi\nu_0] \tag{4}$$

where ν_0 is the bare tune, ψ_i is the phase advance at quadrupole i and $\psi(s)$ is the phase advance at the location where the beta-wave is calculated.

The first order chromatic beta-wave drives the second order chromaticity ξ_2 [2]. The higher order chromaticities are defined by

$$\Delta\nu = \Delta\nu_0 + (\xi_1\delta + \xi_2\delta^2 + \ldots) \tag{5}$$

Chromaticity correction in the Tevatron corrects only the linear chromaticity ξ_1 but not the higher order chromaticities. These higher order terms are significant at low-beta and result in non-linear curves for the tune vs frequency shift during a chromaticity measurement. The second order chromaticity from a sequence of N quadrupoles is [2] is

$$\xi_2 = \frac{1}{8\pi \sin\mu_0} \sum_{i=1}^{N-1} \sum_{j=i+1}^{N} (Q\beta)_i (Q\beta)_j \left(\cos\mu_0 - \cos[2|\psi_j - \psi_i| - 2\pi\nu_0]\right) - \frac{\pi}{2}\cot 2\pi\nu_0 \xi_1^2 - \xi_1 \quad (6)$$

We will use the expressions above to calculate the chromatic beta-wave at the collision points B0 and D0 for the Run II lattice and C0 for the BTeV lattice. For the Run II lattice we will include the contributions from each of the 4 low-beta triplets while for the BTeV lattice we use the 2 triplets around C0.

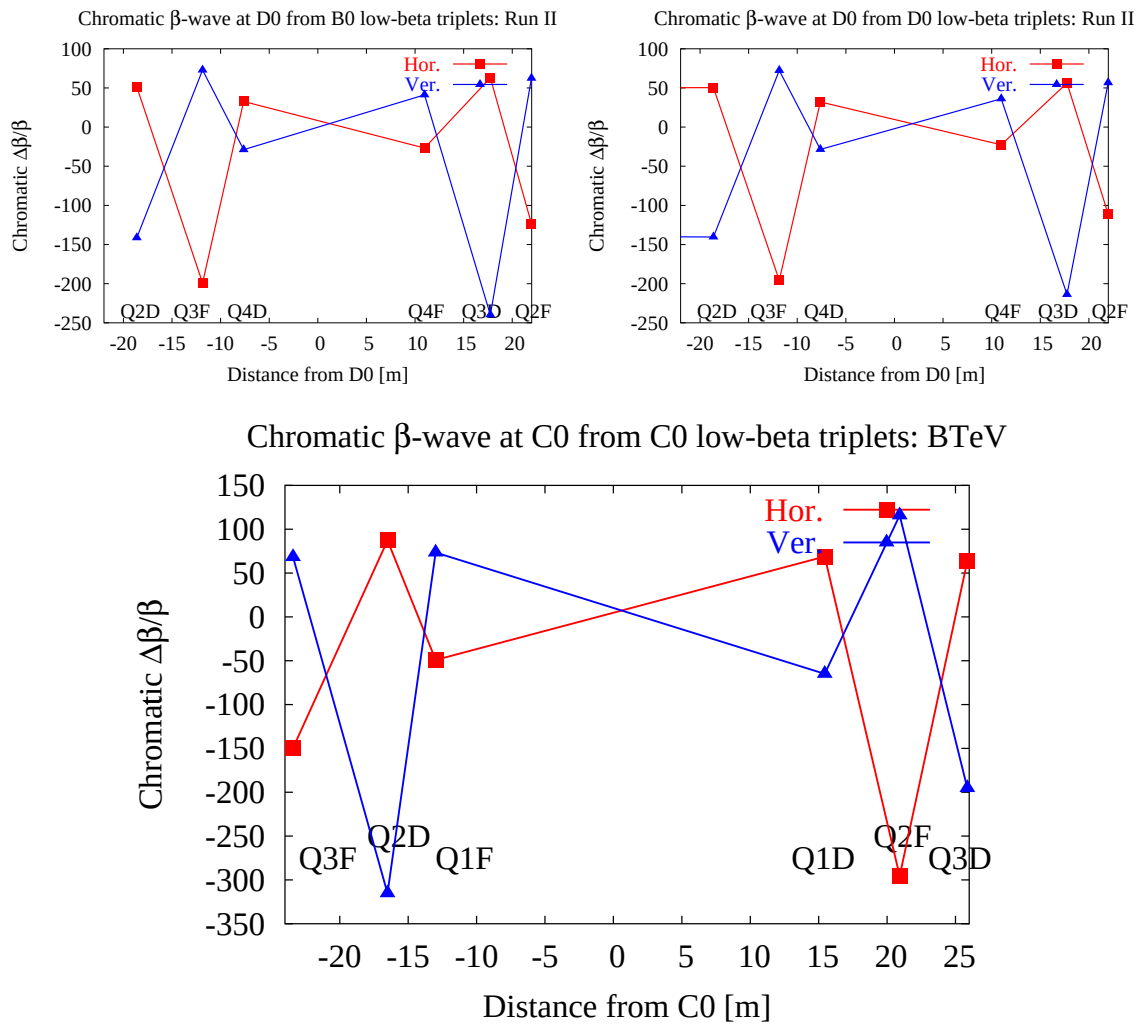

Figure 4: Top Chromatic beta-wave at D0 in the Run II lattice. Left: from the B0 triplets; Top right: from the D0 triplets. Bottom: Chromatic beta-wave at C0 from the C0 triplets in the BTeV lattice.

	Run II		BTeV
	$(\Delta\beta/\beta)_1$ at B0	$(\Delta\beta/\beta)_1$ at D0	$(\Delta\beta/\beta)_1$ at C0
$(\Delta\beta_x/\beta_x)_1$	-384	-393	-274
$(\Delta\beta_y/\beta_y)_1$	-433	-451	-318
	2nd order chromaticity from triplets		
	Run II		BTeV
$(\xi_x)_2$	-6760		-3502
$(\xi_y)_2$	-7849		-4173

Table 2: Linear chromatic beta-wave and 2nd-order chromaticities of the low-beta triplet quadrupoles in Run II and in BTeV.

The plots in Figure 4 show the chromatic beta-wave at D0 from triplet quadrupoles at B0 and D0. Within each triplet, the beta functions reach peak values in quadrupole Q3 so these quadrupoles create the largest beta-wave. The phase advances between B0 and D0 in the two planes are about (27,25) degrees, the beta-wave propagates at twice the phase advance and the beta waves from B0 and D0 at any location add as phasors. The total beta-wave at D0 from the triplets is shown in Table 2. As an example, for particles with a momentum deviation $\delta = 1.4 \times 10^{-4}$, the chromatic beta-wave would lead to a beta change of (5.5, 6.3)% at D0. The chromatic beta-wave at C0 from the C0 triplet in the BTeV lattice is shown in the bottom plot of Figure 4 and the net chromatic beta-wave is shown in Table 2. For comparison, particles with a momentum deviation $\delta = 1.4 \times 10^{-4}$ would suffer a beta change of (3.8, 4.5)% at C0. The second order chromaticities shown in Table 2 are also signicantly smaller in the BTeV lattice. These higher order chromatic effects can excite synchro-betatron resonances, tune modulation etc. which impact the beam lifetime. We expect that such effects will be smaller in the BTeV lattice.

2.3 Emittance growth due to intra-beam scattering

Emittance growth due to intra-beam scattering (IBS) depends on the beam brightness (in six-dimensional phase space) and on the optics in the ring. In the BTeV lattice, optics of the C0 insertion is completely different and the B0 and D0 insertions will not be at the colliding optics. It is therefore possible that the IBS growth rates during collisions will be different than in Run II.

We calculate the growth rates for the Run II and BTeV lattices using the Bjorken-Mtingwa formalism as implemented in MAD. The beam parameters (intensity, emittances etc.) are assumed to be the same for both lattices. We compare these estimates with a simplified IBS theory as developed in Reference [3].

The beam size growth times are defined as

$$\frac{1}{\tau_p} = \frac{1}{\sigma_p}\frac{d\sigma_p}{dt}, \quad \frac{1}{\tau_x} = \frac{1}{\sigma_x}\frac{d\sigma_x}{dt}, \frac{1}{\tau_y} = \frac{1}{\sigma_y}\frac{d\sigma_y}{dt} \tag{7}$$

At high energies the Bjorken-Mtingwa expressions for the growth times can be simplified to the following expressions

$$\begin{aligned} \frac{1}{\tau_p} &= \frac{r_p^2 c N_p (log)}{16\gamma^3(\epsilon_x\epsilon_y)^{3/4}\sigma_s\sigma_p^3}\langle\sigma_H g(\frac{a}{b})(\beta_x\beta_y)^{-1/4}\rangle \\ \frac{1}{\tau_{x,y}} &= \frac{\sigma_p^2\langle\mathcal{H}_{x,y}\rangle}{\epsilon_{x,y}}\frac{1}{\tau_p} \end{aligned} \tag{8}$$

where

$$\begin{aligned} \frac{1}{\sigma_H^2} &= \frac{1}{\sigma_p^2} + \frac{\mathcal{H}_x}{\epsilon_x} + \frac{\mathcal{H}_y}{\epsilon_y} \\ a &= \frac{\sigma_H}{\gamma}\sqrt{\frac{\beta_x}{\epsilon_x}}, \quad b = \frac{\sigma_H}{\gamma}\sqrt{\frac{\beta_x}{\epsilon_x}}, \quad g(\alpha) = \alpha^{[0.021-0.044\ln\alpha]} \\ \mathcal{H}_{x,y} &= \frac{1}{\beta_{x,y}}[D_{x,y}^2 + (\beta_{x,y}D_{x,y}^{'} + \alpha_{x,y}D_{x,y})^2] \\ (log) &\equiv \ln(\frac{b_{max}}{b_{min}}) = \ln(\frac{\sigma_x}{r_p\beta_x/(\gamma^2\epsilon_x)}) \end{aligned} \tag{9}$$

Here $D, D^{'}$ are the dispersion and its slope. The Coulomb logarithm (log) has a value 23.33 in our calculations.

The momentum spread is a key parameter in the growth rates. The "longitudinal temperature" in the center of mass frame of the beam is determined by this spread while the "transverse temperatures" are determined by the beam divergences. Dispersion is another crucial parameter; when the transverse momenta change due to scattering, betatron oscillations are excited and the transverse emittance grows if the dispersion is non-zero. Thus horizontal emittance growth due to IBS is much faster than the vertical emittance growth in the absence of coupling. It should be pointed out that both the Bjorken-Mtingwa and the simplified expressions do not take coupling into account. Typically, coupling equalizes the growth rates in the two transverse planes. We will assume that to be the case in the following.

Energy[GeV]	980
Bunch intensity	2.7×10^{11}
Hor. emittance (95%) [π-mm-mrad]	20
Ver. emittance (95%) [π-mm-mrad]	20
RMS Bunch length [m]	0.60
RMS Momentum spread	1.4×10^{-4}

Table 3: Proton beam parameters assumed for the IBS calculations

	Run II	BTEV
$\langle\beta_x\rangle$	71.66	69.06
$\langle\beta_y\rangle$	71.94	68.60
$\langle D_x\rangle$	2.84	2.71
$\langle D_y\rangle$	-3.5×10^{-3}	4.2×10^{-3}
$\langle\mathcal{H}_x\rangle$	0.20	0.18
$\langle\mathcal{H}_y\rangle$	5.8×10^{-4}	4.9×10^{-4}

Table 4: Average values of optics functions in the two lattices.

Table 3 shows the key beam parameters assumed for the IBS calculations for both the Run II and BTeV lattices.

Table 4 shows the average values of some of the optics functions in the two lattices. The average optics functions have slightly smaller values in the BTeV lattice because there is only a single low-beta insertion. Based on these average values, we can make some informed guesses about the differences in the IBS growth rates in the two lattices. If we make the crude approximations of replacing the average of products in the growth rates by the product of averages and similar approximations, we can write the change in the longitudinal growth time τ_p due to changes in the beta functions as

$$\frac{\Delta\tau_p}{\tau_p} = \frac{1}{4}[\langle\frac{\Delta\beta_x}{\beta_x} + \frac{\Delta\beta_y}{\beta_y}\rangle] \tag{10}$$

Here we have also assumed that the changes in beta functions are small enough that they do not change the parameter σ_H, which is close to the value of the rms momentum spread σ_p. Thus the longitudinal growth time will be larger (or growth rate slower) in a lattice with larger beta functions.

This can be understood by the following intuitive argument. The IBS growth rates are determined by thermal equilibrium in the center of mass (CM) frame: the coldest plane grows the fastest. The temperatures in the CM frame are proportional to the momenta in this frame. A particle with an rms momentum deviation σ_p in the lab frame has a longitudinal momentum $p_s = p_0\sigma_p/\gamma$ in the CM frame while the horizontal momentum for a particle with the rms slope, $x' = \sigma_{x'} = \sqrt{\epsilon_x^N/\gamma\beta_x}$ is $p_x = p_0\sigma_{x'}$. Hence the ratio of the longitudinal to horizontal temperature is

$$\frac{T_p}{T_x} = \frac{p_s^2}{p_x^2} = \frac{\beta_x}{\gamma\epsilon_x^N}\sigma_p^2 \tag{11}$$

	MAD (Bjorken-Mtingwa)		Bane's approx. [3]	
	Run II	BTeV	Run II	BTeV
τ_p [hrs]	26.4	25.4	26.2	25.4
τ_x [hrs]	23.6	25.4	20.8	23.1
τ_y [hrs]	neg.	neg.	7308	8531

Table 5: IBS beam size growth times for Run II and BTeV at 980 GeV

Thus if the beta function increases, the longitudinal temperature increases relative to the transverse temperature and the longitudinal growth slows down.

The above qualitative arguments have been followed up with the calculations of the growth rates using the BM formulation with MAD and also with Bane's approximation [3]. Table 5 shows the beam size growth times obtained for protons on the proton helix from MAD and the simplified expressions. Note that MAD calculates the emittance growth times, so those numbers are doubled to determine the beam size growth times. First we note that both calculations show that in the BTeV lattice, the longitudinal growth will be slightly faster but the transverse growth will be somewhat slower - as expected from qualitative arguments. The differences are however less than 10%. Thus we expect that BTeV optics will not cause any major changes to the beam emittance growth.

We observe that the longitudinal growth time found from the approximate expressions agree quite closely with the more exact Bjorken-Mtingwa calculation. The approximate horizontal growth time is within 10% of the B-M results. As pointed out above, coupling will transfer thermal energy between the two transverse planes. Without coupling the horizontal beam size growth is expected to be around 4%/hr while in the extreme of full coupling, both horizontal and vertical beam sizes are expected to grow at around 2%/hr.

3 Beam-beam effects

The fact that there is only a single experiment in the BTeV lattice reduces the tune footprint from the head-on beam-beam interactions by a factor of two, all other things being equal. The impact of the long-range interactions is determined mainly by the helix configuration. Figure 5 shows the beam separation at all interactions in units of the rms beam size for Run II and BTeV. The average separation is larger in BTeV, the minimum separation is $\sim 6\sigma$ and occurs at one location. On the other hand, in Run II separations close to 5σ occur at several interactions. We therefore expect the beam-beam interactions to have a smaller impact on beam quality in the BTeV lattice. We now quantify the impact of the beam-

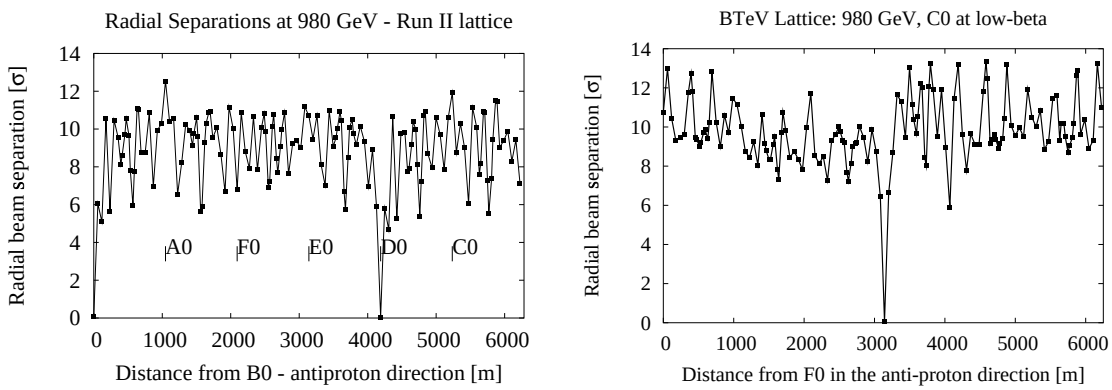

Figure 5: Beam separation at 980 GeV in units of the rms proton beam size; Left: Run II, Right: BTeV CDR1 lattice

beam interactions by detailed calculations. The beam-beam interactions change the tunes, coupling, chromaticities and resonance strengths. Analytical expressions of these amplitude dependent quantities can be found in Reference [4]. We can illustrate the dependence of these quantities on beam parameters by writing the expressions for round beams at zero amplitude,

$$\Delta\nu_x(0,0) = \frac{N_p r_p}{2\pi\epsilon_p^N}\frac{\cos 2\theta}{d^2} \tag{12}$$

$$F_{1,-1,p}(0,0) = -\frac{N_p r_p}{\pi\epsilon_p^N}\frac{\sin 2\theta}{d^2}\exp[i(\psi_x - \psi_y - (\nu_x - \nu_y - p)\frac{s}{R})] \tag{13}$$

$$\nu'_x(0,0) = 2\frac{N_p r_p}{\pi\epsilon_p^N}\frac{1}{d^3}[\tilde{\eta}_x\cos 3\theta + \tilde{\eta}_y \sin 3\theta] \tag{14}$$

Here N_p is the proton bunch intensity, r_p is the classical proton radius, ϵ_p^N is the normalized proton emittance, θ is the angle of the plane of the helix, d is the beam separation in units of the rms proton beam size, ψ_x, ψ_y are the phase advances, ν_x, ν_y are the tunes and $\tilde{\eta}_x, \tilde{\eta}_y$ are the dispersions in units of the rms beam sizes. At large distances, both the tune shift and the coupling fall as $1/d^2$ while the chromaticity falls off more rapidly as $1/d^3$. These optical parameters have different dependencies on the helix angle θ. For example at 45°, the tune shift vanishes but the coupling is a maximum. If the vertical dispersion is zero, the chromaticity vanishes only if $\theta = 30°, 90°$.

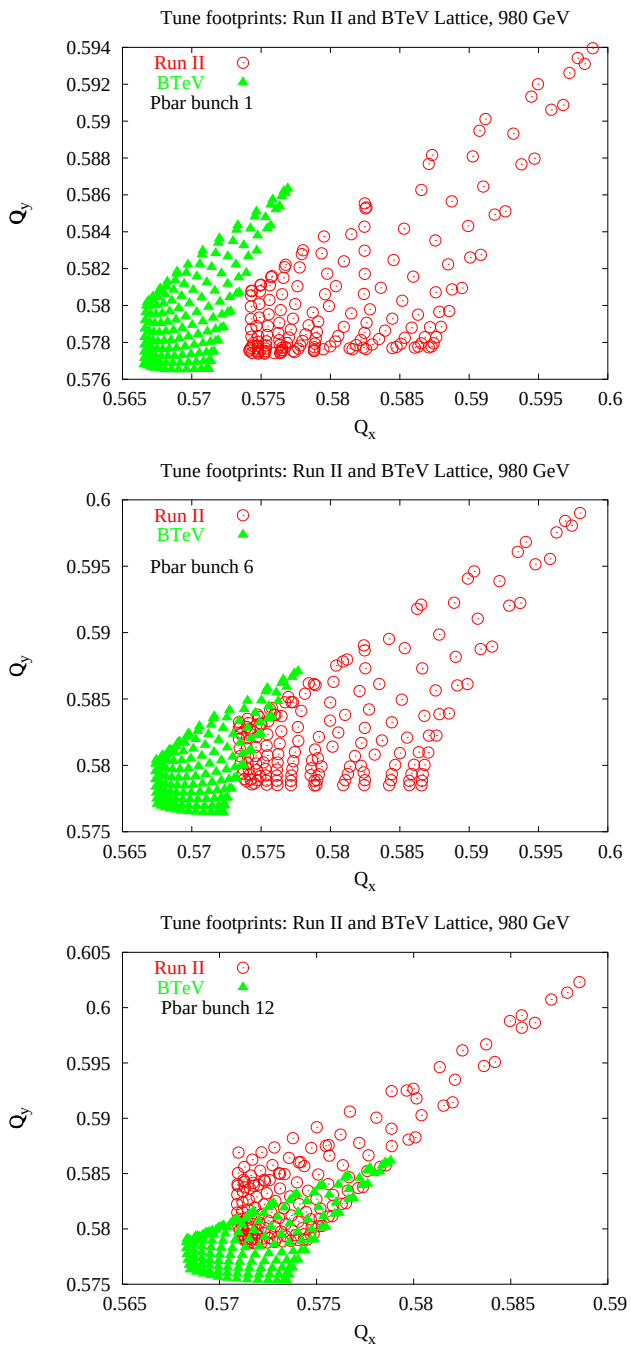

Figure 6: Tune footprints of antiproton bunches 1, 6 and 12 in the two lattices. The tunes on the antiproton helix and without beam-beam interactions have been adjusted to the same values.

The amplitude dependent tunes (tune footprint) from beam-beam interactions can be calculated analytically or by tracking. We wish to include the machine nonlinearities since their contribution changes from Run II to BTeV, hence we use tracking. Footprints of 3 representative bunches are compared for Run II and BTeV in Figure 6. The working points have been adjusted to have the same values in both lattices on the anti-proton helix in the absence of beam-beam interactions. The footprints extend from 0 to 6 σ in all cases, the small amplitude particles are to the upper right of the footprint. As expected, the tune footprint is about a factor of two smaller in BTeV. We also note that the tune shifts of the (6,6) σ particles are also larger in Run II. Figure 3 shows the footprints of the representative bunches in BTeV. Compared to Figure 6, the working point has been shifted to a different value. The tune footprints in BTeV are small enough to fit into the resonance free space between the 7th and 12th order resonances.

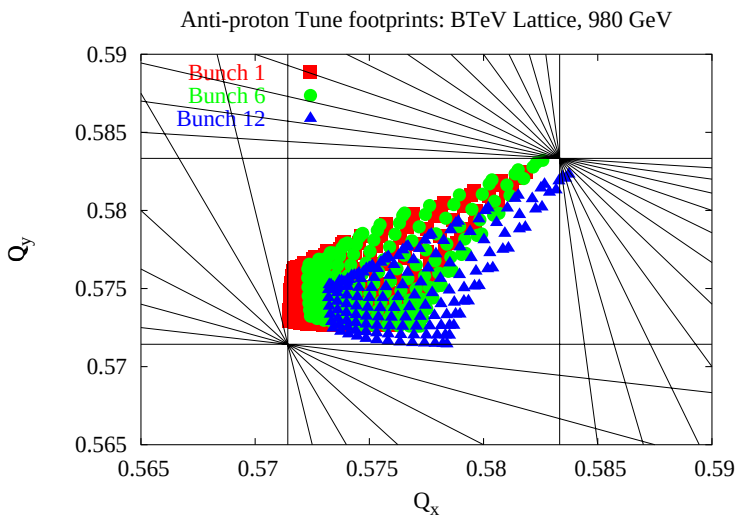

Figure 7: Tune footprints of anti-proton bunches 1, 6 and 12 in BTeV. The footprints fit in the resonance free space between the 7th and 12th order resonances.

Using the exact expressions [4] for elliptical beams, we have evaluated the zero amplitude tune shifts, chromaticities and minimum tune shifts for each of the 12 anti-proton bunches in a train. These quantities are shown in Figures 8, 9, and 10, respectively. The zero amplitude tune shifts are a about a factor of two smaller in BTeV. The vertical tune shifts are systematically larger than the horizontal for every anti-proton bunch except bunch 12 in BTeV - the reason is discussed later in Figure 11. Small amplitude chromaticities, seen in Figure 9, are reduced by about a factor of two in the horizontal plane in BTeV. The much smaller vertical chromaticities are about the same in both lattices. Figure 10 shows the small amplitude minimum tune split, a measure of the coupling. The coupling due to these beam-beam interactions is nearly 3-4 times larger in BTeV than in Run II. These values for BTeV are not a major source of concern but there is room for improvement.

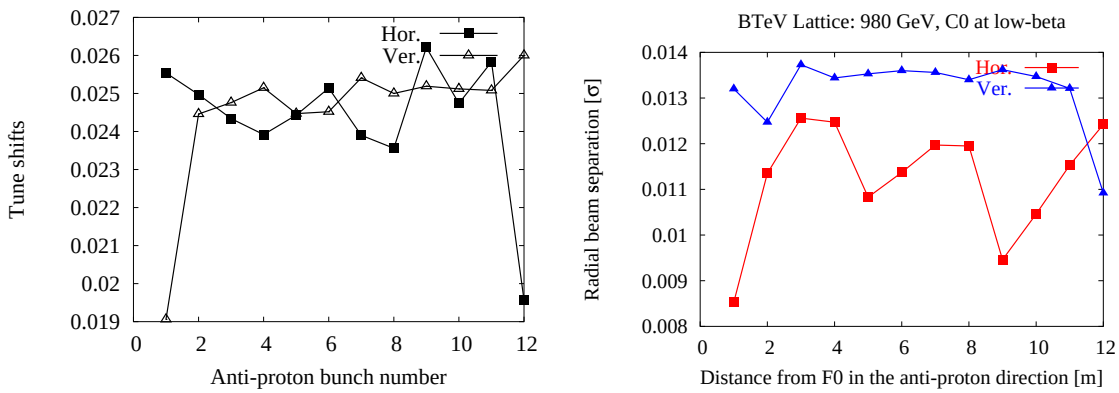

Figure 8: Small amplitude tune shifts, bunch by bunch. Left: Run II lattice, Right: BTeV lattice

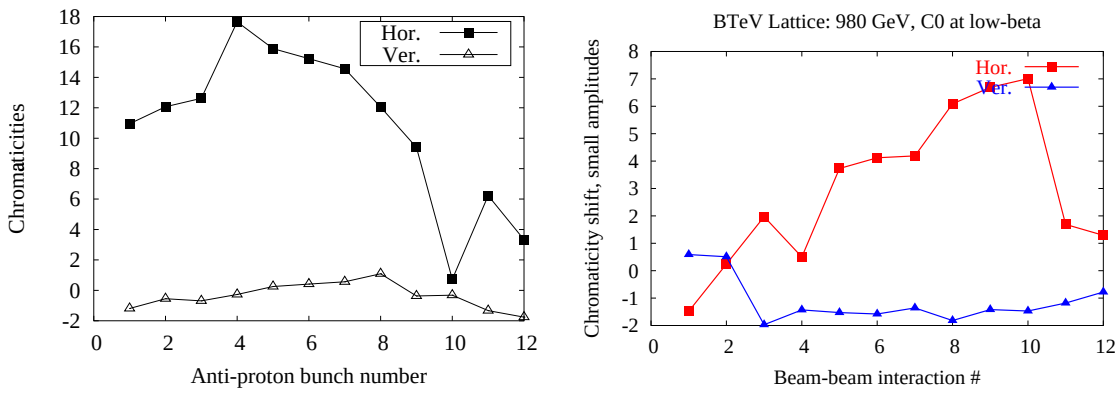

Figure 9: Small amplitude chromaticity shifts, bunch by bunch. Left: Run II lattice, Right: BTeV lattice

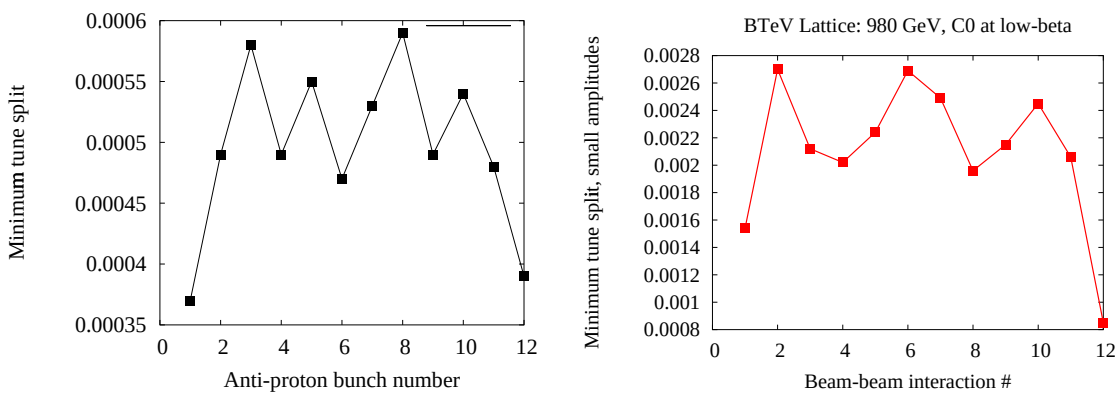

Figure 10: Small amplitude minimum tune split, bunch by bunch. Left: Run II lattice, Right: BTeV lattice

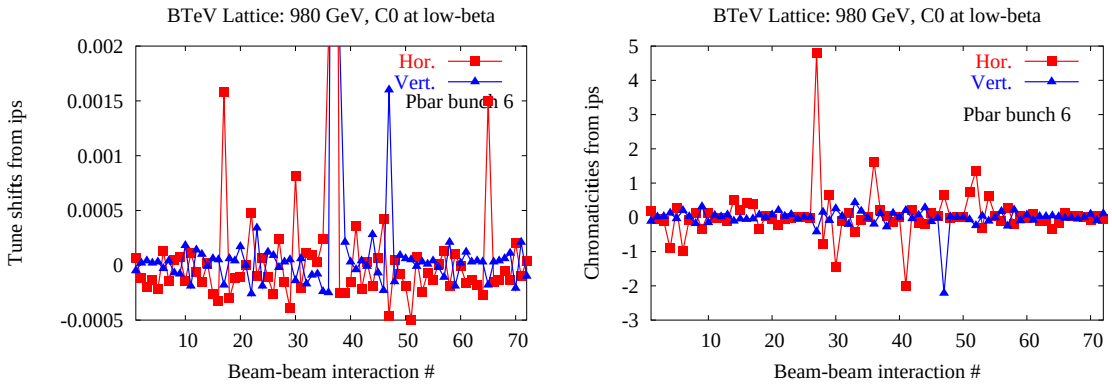

Figure 11: Left: Small amplitude tune shifts from each beam-beam interaction for anti-proton bunch 6. The contributions from the head-on collisions at C0 (interaction #37) are off-scale in this plot. Right: Small amplitude chromaticities from each beam-beam interaction for anti-proton bunch 6.

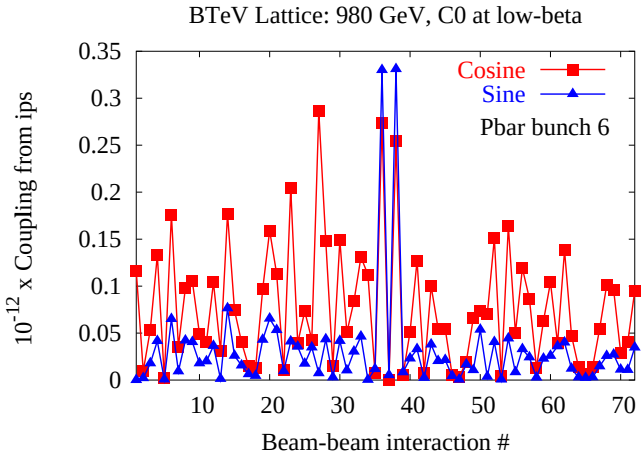

Figure 12: Small amplitude coupling resonance terms from each beam-beam interaction for anti-proton bunch 6.

It is useful to identify the contributions from individual beam-beam interactions. This can help make targeted changes to the optics and the helix. Figure 11 shows the zero amplitude tune shifts from each of the interactions for anti-proton bunch 6. The contribution from the head-on collisions is off-scale in this figure. There are two parasitics which contribute a relatively large positive horizontal tune shift and one parasitic that contributes a relatively large positive vertical tune shift. However there are several more parasitics that contribute negative horizontal tune shifts. As a consequence the net tune shift is smaller in the horizontal plane, as seen in Figure 8. Figure 11 also shows the chromaticities from individual interactions, also for bunch 6. This identifies interaction # 27 (where $\beta_x = 129$m, dispersion D_x=5.5m) as the largest contributor to the chromaticity. The coupling contributions can be seen in Figure 12 where we plot the cosine and sine terms of the linear coupling resonance. The contributions from the two parasitics nearest to C0 dominate. Changes in the optics have reduced the coupling in the present version of the BTeV design compared to an earlier

optics design. Changes to the helix may help in reducing this coupling further.

We now turn to a discussion of the nonlinear resonances driven by the beam-beam interactions. The rather complicated expressions for the resonance driving terms may be found in reference [4]. We consider the 5th and 7th order resonances, the lowest order resonances that are closest to the usual working point. The resonance terms vary with amplitude, increasing from the origin, reaching a maximum at some amplitude before decreasing to zero at large amplitudes. We choose an amplitude of 6σ for our comparisons. Figure 13 shows the amplitude of the resonance driving terms for anti-proton bunches 1, 6 and 12 for the two lattices. Of the six 5th order resonances, only one is larger in BTeV for each bunch. The majority are smaller in BTeV by more than a factor of two. The relative strengths of the 7th order resonances show greater variation in the two lattices. Considering for example bunch 6 in the middle of the train, three of the eight 7th order resonances are smaller in BTeV, three are comparable while one is larger. From these 7th order resonances alone, it is hard to draw a conclusion about the relative strengths of the beam-beam interactions in the two lattices.

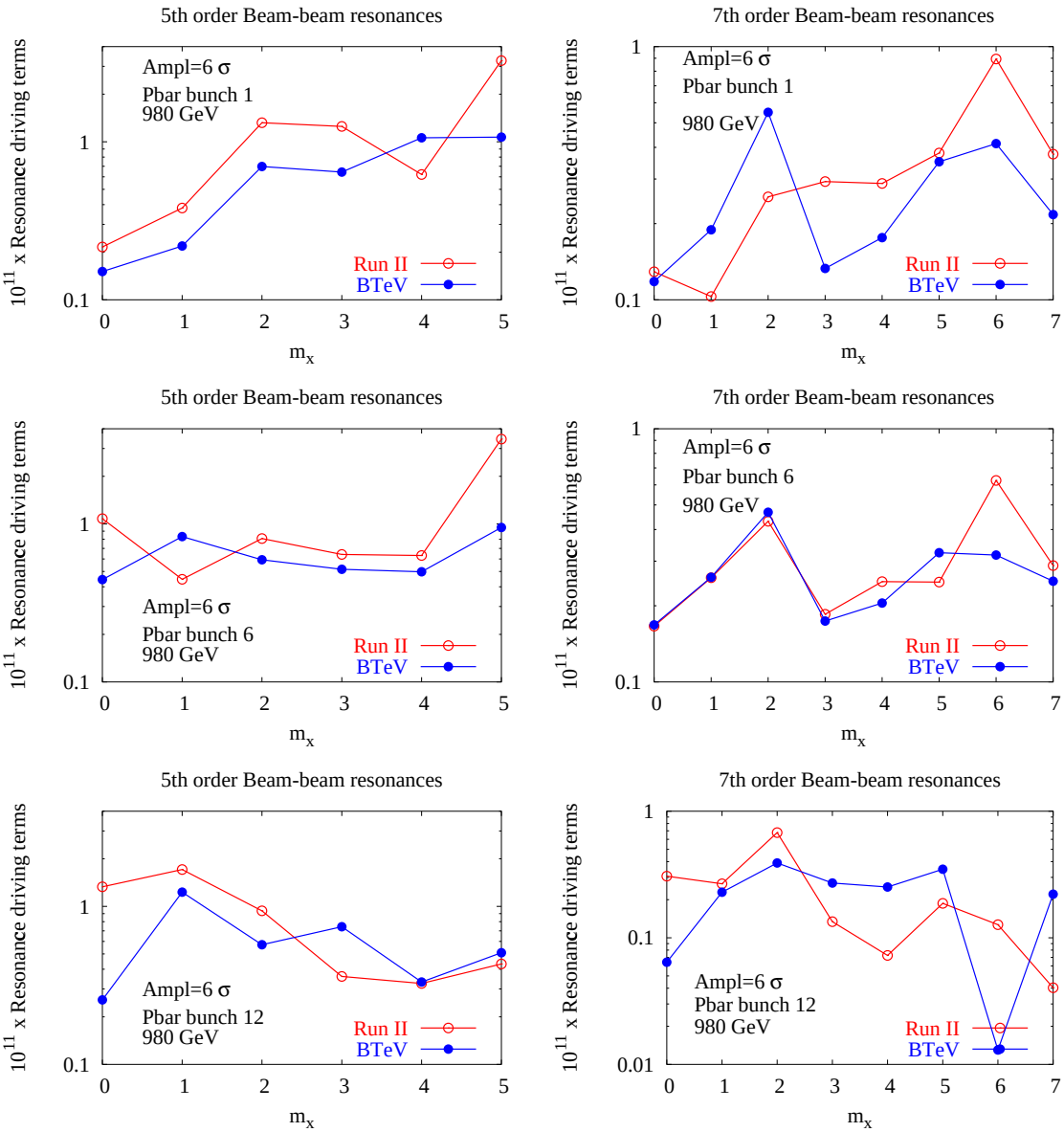

Figure 13: Comparison of 5th (left) and 7th order (right) resonance driving terms for the Run II lattice and the BTeV lattice for anti-proton bunch 1 (top), bunch 6 (middle) and bunch 12 (bottom). The horizontal axis labels the resonance $m_x\nu_x + (n - m_x)\nu_y = p$ where n is the order of the resonance.

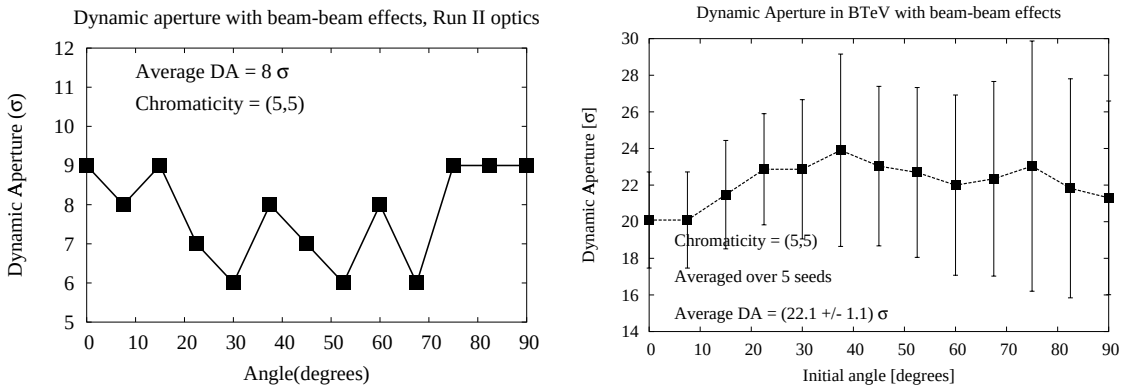

Figure 14: Dynamic Aperture with beam-beam effects. Left: Run II, Right: BTeV

3.1 Dynamic Aperture

The dynamic aperture (DA) has been calculated with the same set of lattice errors reported earlier in Section 2.1 but with the inclusion of the beam-beam interactions. Figure 14 shows the dynamic aperture in Run II and BTeV. Comparing these values to the dynamic apertures without beam-beam interactions, shown in Figure 3, we observe that the beam-beam interactions in Run II reduce the DA by 5σ from 13σ to 8σ while the beam-beam interactions in BTeV reduce the DA from 24σ to 22σ. Earlier simulations [5] had shown that the head-on interactions have a negligible impact on the DA. We conclude that the smaller reduction of the DA in BTeV is due to the reduced impact of the long-range interactions.

3.2 Diffusion and emittance growth due to the beam-beam interactions

Analytical calculations of resonance driving terms and dynamic aperture simulations have predicted that beam-beam effects will not be as strong in the BTeV lattice. The weaker nonlinearities should have a direct impact on observable quantities such as diffusion, emittance growth and beam lifetimes. We have used multi-particle simulations to calculate these quantities using the code BBSIM developed at FNAL. The simulation model includes the beam-beam interactions (head-on and long-range) with linear transport between the interactions. Effects due to machine nonlinearities are not included.

We calculate diffusion coefficients as follows. For example, the horizontal diffusion coefficient at an amplitude A after N turns is

$$DJ_x(A) = \frac{1}{N}\langle\langle\Delta[\mathrm{Var}J_x(A)]\rangle\rangle \tag{15}$$

where $\Delta[\mathrm{Var}J_x(A)]$ is the change in the variance of the horizontal action. The double average $\langle\langle\rangle\rangle$ signifies two averages: the action at each turn is first averaged over 100 particles placed at each amplitude and then a second average is taken every 1000 turns (about 2 synchrotron periods) to eliminate short term amplitude beating from phase space distortions. The variance of this averaged action is calculated. The diffusion coefficient at each amplitude thus calculated typically converges after about a million turns.

Figure 15 shows the horizontal and vertical diffusion coefficients for the two lattices at several amplitudes. At amplitudes between 3-5 σ, the coefficients in BTeV are smaller by

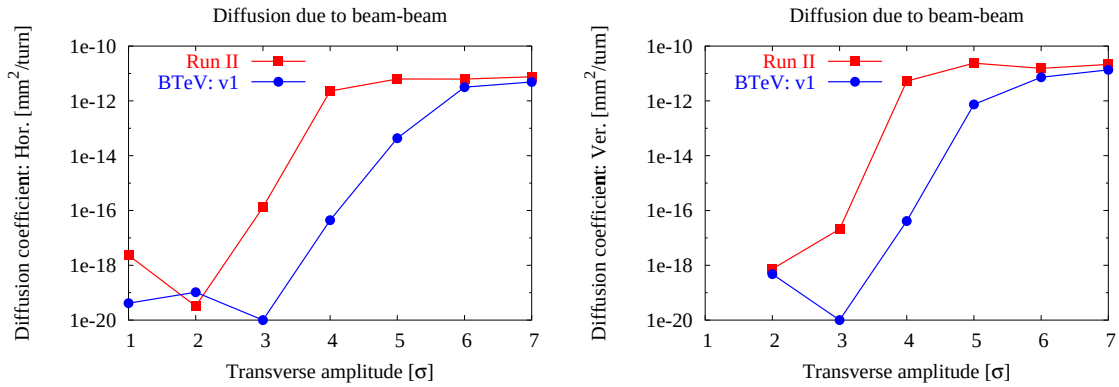

Figure 15: Diffusion at several amplitudes due to the beam-beam interactions in the Run II and BTeV lattices.

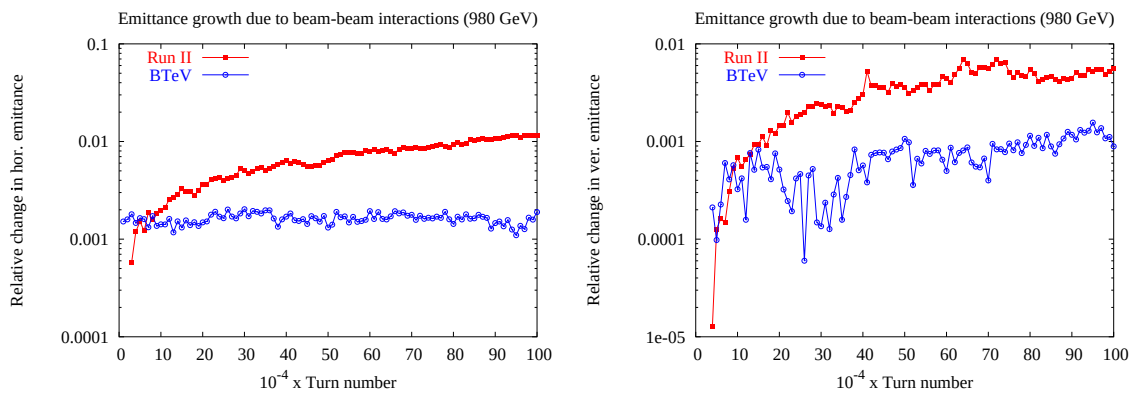

Figure 16: Relative change in the horizontal and vertical emittances of anti-protons in the Run II and BTeV lattices.

an order of magnitude or more. This implies that the transverse beam tails will grow more slowly in the BTeV lattice.

We have also calculated the emittance growth in both lattices by tracking 2×10^4 particles for 10^6 turns. Figure 16 shows the statistical emittances within a 3σ envelope for the two cases. Again, emittance growth in BTeV is about an order of magnitude less and is at the level of statistical noise in these simulations. These simulations of diffusion and emittance growth are therefore consistent with the expectation that nonlinear effects due to beam-beam effects will be weaker in the BTeV lattice.

3.3 Orbit changes and relative luminosities

The long-range interactions change the orbits, hence each bunch will have a slightly different offset at the collision point. These offsets and the resulting loss in luminosity can be calculated from a knowledge of the optics. Figure 17 compares the bunch by bunch offsets at B0 (as an example) in Run II and at C0 in BTeV. The maximum offset at B0 is about 1μm but is nearly 3.5μm at C0. The likely explanation for the larger offsets is that the phase advances from the different parasitics to C0 are such that the orbit shifts add more coherently that

they do for the net orbit shift at B0.

The single bunch luminosity of beams that are offset by $(\Delta x, \Delta y)$ at the IP is given by

$$\mathcal{L} = \frac{N_p N_{pbar} f_{rev}}{\pi} \frac{1}{\sqrt{(\epsilon_{x;p} + \epsilon_{x;pbar})(\epsilon_{y;p} + \epsilon_{y;pbar})}} \frac{1}{\sqrt{\pi}\sigma_{z;eff}} \int_0^\infty \frac{dt}{1+t^2} \exp[-t^2 z^2 - \frac{\Delta x^2}{4\sigma_{x;h}^2} - \frac{\Delta y^2}{4\sigma_{y;h}^2}] \tag{16}$$

where

$$\begin{aligned} z &= \frac{\beta^*}{\sigma_{z;eff}}, \qquad \sigma_{z;eff}^2 = \frac{1}{2}(\sigma_{z;p}^2 + \sigma_{z;pbar}^2) \\ \sigma_{x;h}^2 &= \frac{1}{2}\beta^*(\epsilon_{x;p} + \epsilon_{x;pbar})[1+t^2], \quad \sigma_{y;h}^2 = \frac{1}{2}\beta^*(\epsilon_{y;p} + \epsilon_{y;pbar})[1+t^2] \end{aligned} \tag{17}$$

Here we have assumed the beams are round but not necessarily the same size at the IPs. The impact of these offsets on the luminosity variation bunch to bunch is negligibly small in Run II, less than 0.01%. The bunch to bunch luminosity variation in BTeV, seen in Figure 18, is somewhat larger but still negligible compared to variations from other sources such as intensity and emittance variations.

3.4 Beam-beam effects on protons

There is strong evidence that proton losses at the start of stores in Run II are driven by the head-on collisions at B0 and D0. These losses are tune dependent and are larger when the anti-proton transverse beam size (especially in the vertical plane) is smaller than the proton beam size. Proton losses have been reduced to tolerable levels by changing the proton working point to lie between the 7th and 12th order resonances.

When proton beam sizes are larger, protons experience the largest nonlinearity of the beam-beam force at the edge of the anti-proton beam. Diffusion drives the protons to the physical aperture and nearness to resonances enhances the diffusion. This is a qualitative explanation of the phenomena but a quantitative model which explains the observations in greater detail does not yet exist.

There will be head-on collisions at only a single experiment in BTeV. Hence losses due to head-on collisions will be smaller. Nevertheless, with higher anti-proton intensities than at present, proton losses will need to be carefully monitored. Operational solutions found at the end of Run II might well suffice for BTeV.

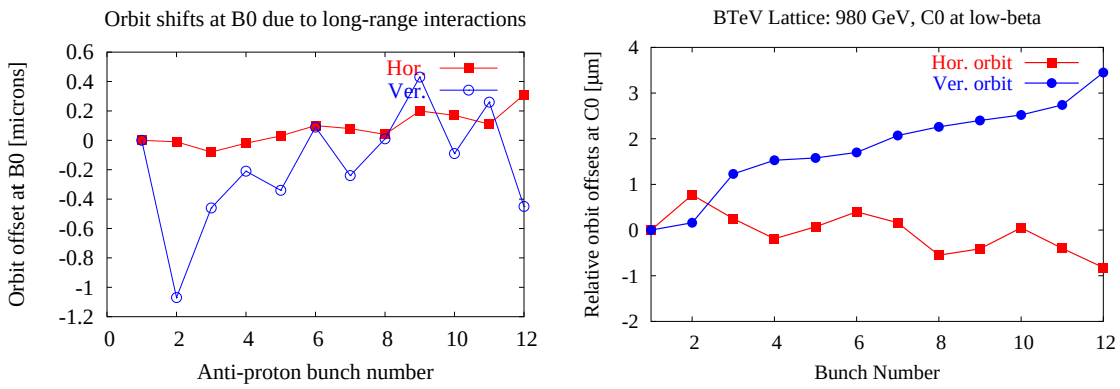

Figure 17: Bunch by bunch orbit shifts due to the long-range interactions; left: At B0 in Run II, right: At C0 in BTeV. The shifts are calculated relative to the first bunch.

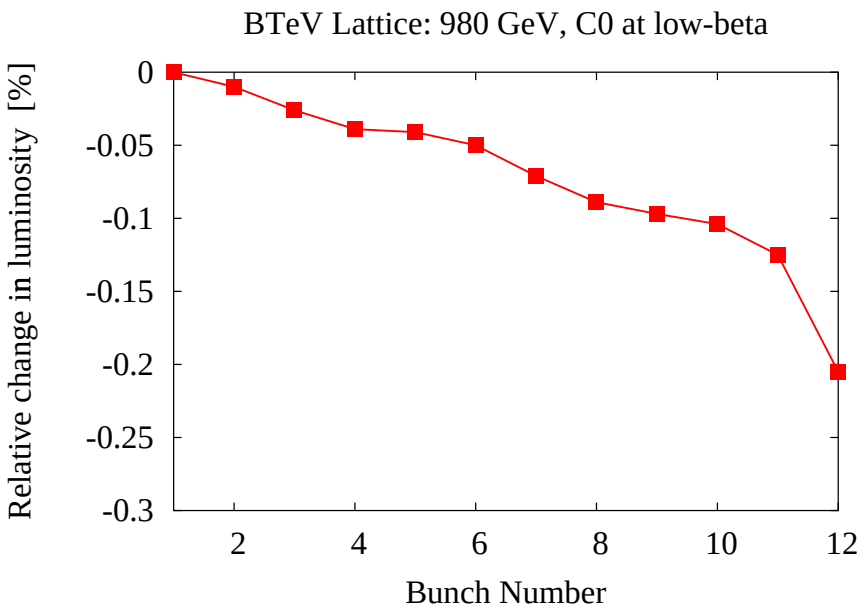

Figure 18: Relative changes in luminosity bunch by bunch due to the long-range interactions. The first bunch in each beam is assumed to be perfectly centered at C0.

4 Beam and Luminosity Lifetimes

In this section we will estimate intensity and luminosity lifetimes in BTeV using data from the record luminosity store 3637 on July 16, 2004 when the average initial luminosity exceeded $1 \times 10^{32}\text{cm}^{-2}\text{sec}^{-1}$. Table 6 shows some of the relevant parameters for this store.

Average initial luminosity [$\text{cm}^{-2}\text{sec}^{-1}$]	1.03×10^{32}
Average luminosity lifetime [hrs]	7.81
Proton beam intensity after halo removal	8848×10^{9}
Proton lifetime during first 2 hrs in the store [hrs]	45.7
Anti-proton beam intensity after halo removal	1556×10^{9}
Anti-proton lifetime during first 2 hrs in the store [hrs]	24.3
Effective emittance from luminosity [πmm-mrad]	17.1
Proton bunch length at low-beta [nsec]	1.6
Anti-proton bunch length at low-beta [nsec]	1.63

Table 6: Selected beam parameters during the record store 3637 on July 16, 2004

The peak luminosity in BTeV is assumed to be $2\times10^{32}\text{cm}^{-2}\text{sec}^{-1}$. We will assume that this luminosity is attained by increasing the anti-proton intensity, all other beam parameters are assumed to be the same. Table 7 shows our assumptions for BTeV.

The luminosity, assuming the beams are perfectly centered, can be written as

$$\mathcal{L} = \frac{3\gamma f_{rev} M_b N_p N_{\bar{p}}}{2\pi\beta^* \epsilon_{\perp,eff}} \mathcal{H}(\frac{\beta^*}{\sigma_{s,eff}}) \tag{18}$$

where M_b is the number of bunches, N_p is the proton bunch intensity, $N_{\bar{p}}$ is the anti-proton bunch intensity, $\epsilon_{\perp,eff}$ the 95% effective emittance of the beams and $\mathcal{H}$ is the hourglass form factor

$$\mathcal{H}(z) = \sqrt{\pi} z e^{z^2}(1-\Phi(z)), \qquad \Phi(z) = \frac{2}{\sqrt{\pi}} \int_0^z e^{-t^2} dt \tag{19}$$

Intensity losses, transverse and longitudinal emittance growth all contribute to the decay in luminosity. The luminosity lifetime is

$$\frac{1}{\tau_{\mathcal{L}}} = \frac{1}{\tau_p} + \frac{1}{\tau_{\bar{p}}} + \frac{1}{\tau_{\epsilon_{\perp,eff}}} + (1 - \frac{2z}{\mathcal{H}} + 2z^2)\frac{1}{\tau_{s,eff}} \tag{20}$$

where

$$\frac{1}{\tau_{\mathcal{L}}} = -\frac{1}{\mathcal{L}}\frac{d\mathcal{L}}{dt}, \quad \frac{1}{\tau_p} = -\frac{1}{N_p}\frac{dN_p}{dt}, \quad \frac{1}{\tau_{\bar{p}}} = -\frac{1}{N_{\bar{p}}}\frac{dN_{\bar{p}}}{dt}, \quad \frac{1}{\tau_{\epsilon_{\perp,eff}}} = \frac{1}{\epsilon_{\perp,eff}}\frac{d}{dt}\epsilon_{\perp,eff}, \quad \frac{1}{\tau_{s,eff}} = \frac{1}{\sigma_{s,eff}}\frac{d}{dt}\sigma_{s,eff} \tag{21}$$

Peak luminosity [$\text{cm}^{-2}\text{sec}^{-1}$]	2×10^{32}
Proton beam intensity	$36 \times 2.7 \times 10^{11}$
Anti-proton beam intensity	$36 \times 1 \times 10^{11}$

Table 7: Assumed parameters for BTeV

We define now an effective emittance growth time which includes both transverse and longitudinal effects,

$$\frac{1}{\tau_{\epsilon,eff}} \equiv \frac{1}{\tau_{\epsilon_{\perp},eff}} + (1 - \frac{2z}{\mathcal{H}} + 2z^2)\frac{1}{\tau_{s,eff}} \tag{22}$$

Intra-beam scattering (IBS), rf noise, residual gas scattering, machine nonlinearities, ... are the main contributors to $\tau_{\epsilon,eff}$. During a store these growth times are measured by the synchrotron light monitor but these measured values are not yet reliable enough to be used with confidence. The measured luminosity and intensity lifetimes are more credible so we calculate $\tau_{\epsilon,eff}$ from these lifetimes as

$$\frac{1}{\tau_{\epsilon,eff}} = \frac{1}{\tau_{\mathcal{L}}} - \frac{1}{\tau_p} - \frac{1}{\tau_{\bar{p}}} \tag{23}$$

Transverse and longitudinal emittance growth of protons due to IBS contribute the most to $\tau_{\epsilon,eff}$. We saw earlier in Section 2.3 that IBS growth times for protons are about the same in BTeV as in Run II. The anti-proton growth times will be smaller in BTeV due to increased intensities. However with an intensity ratio 2.7(protons):1(anti-protons), we expect the emittance growth times to not change significantly in BTeV. We assume therefore that

$$\tau_{\epsilon,eff}|_{BTeV} = \tau_{\epsilon,eff}|_{RunII} \tag{24}$$

Inelastic scattering at the experiments and dynamics (beam-beam, machine nonlinearities, IBS, rf noise, ...) contribute to the intensity losses. We can calculate the intensity lifetime due to dynamics from the measured intensity lifetime as

$$\frac{1}{\tau_p(Dy)} \equiv \frac{1}{\tau_p} - \frac{1}{\tau_p(\mathcal{L})}, \quad \frac{1}{\tau_{\bar{p}}(Dy)} \equiv \frac{1}{\tau_{\bar{p}}} - \frac{1}{\tau_{\bar{p}}(\mathcal{L})}, \tag{25}$$

$$\frac{1}{\tau_p(\mathcal{L})} = \frac{N_{IP}M_bN_p}{\mathcal{L}\sigma_{p\bar{p}}}, \quad \frac{1}{\tau_{\bar{p}}(\mathcal{L})} = \frac{N_{IP}M_bN_{\bar{p}}}{\mathcal{L}\sigma_{p\bar{p}}} \tag{26}$$

where N_{IP} is the number of experiments. The scattering cross-section $\sigma_{p\bar{p}} = 70$ mbarns. If beam-beam effects are the dominant contributors to dynamic losses, then from our calculations in Section 3 we expect that $\tau(Dy)$ will be larger for both beams in BTeV. For the sake of simplicity we assume

$$\tau_p(Dy)|_{BTeV} = \tau_p(Dy)|_{RunII}, \quad \tau_{\bar{p}}(Dy)|_{BTeV} = \tau_{\bar{p}}(Dy)|_{RunII} \tag{27}$$

This is a conservative assumption but one that should put a lower bound on our lifetime estimates for BTeV.

Now let's put in some numbers. From the values in Table 6 for Store 3637 and the above definitions we find the following lifetimes for this store. We will take these values to be representative for Run II. The dynamic lifetimes of protons is about half that of anti-protons showing that beam-beam phenomena and other processes have a stronger impact on protons during this store. There is evidence that the head-on collisions at B0 and D0 are responsible for much of the proton losses related to beam-beam interactions. Therefore one could argue that even with higher anti-proton intensities in BTeV but only one experiment, the dynamic proton losses may not be significantly different from Run II losses. The emittance growth

	From Luminosity	From Dynamics	Total
Proton lifetime [hrs]	170	62	46
Anti-proton lifetime [hrs]	30	128	24
$\tau_{\epsilon,eff}$ [hrs]	15		

Table 8: Intensity lifetimes and (tranverse, longitudinal) emittance growth time $\tau_{\epsilon,eff}$ defined in Equation 22 calculated for Store 3637. These values are taken to be representative of Run II.

	From Luminosity	From Dynamics	Total (BTeV)
Proton lifetime [hrs]	192	62	47
Anti-proton lifetime [hrs]	71	128	46
$\tau_{\epsilon,eff}$ [hrs]	15		
Luminosity lifetime [hrs]	9		

Table 9: Intensity and luminosity lifetime estimates for BTeV

time $\tau_{\epsilon,eff}$ is comparable to the longitudinal and transverse emittance growth times due to IBS calculated in Section 2.3.

With our assumptions of beam parameters for BTeV shown in Table 7, we calculate the intensity and luminosity lifetimes. Under our assumptions we have

$$\frac{1}{\tau_p|_{BTeV}} = \frac{1}{\tau_p(\mathcal{L})|_{BTeV}} + \frac{1}{\tau_p(Dy)|_{BTeV}} = \frac{1}{\tau_p(\mathcal{L})|_{BTeV}} + \frac{1}{\tau_p(Dy)|_{RunII}} \tag{28}$$

$$\frac{1}{\tau_{\bar{p}}|_{BTeV}} = \frac{1}{\tau_{\bar{p}}(\mathcal{L})|_{BTeV}} + \frac{1}{\tau_{\bar{p}}(Dy)|_{BTeV}} = \frac{1}{\tau_{\bar{p}}(\mathcal{L})|_{BTeV}} + \frac{1}{\tau_{\bar{p}}(Dy)|_{RunII}} \tag{29}$$

$$\frac{1}{\tau_{\mathcal{L}}|_{BTeV}} = \frac{1}{\tau_p|_{BTeV}} + \frac{1}{\tau_{\bar{p}}|_{BTeV}} + \frac{1}{\tau_{\epsilon,eff}|_{BTeV}} = \frac{1}{\tau_p|_{BTeV}} + \frac{1}{\tau_{\bar{p}}|_{BTeV}} + \frac{1}{\tau_{\epsilon,eff}|_{RunII}} \tag{30}$$

Table 9 shows the intensity and luminosity lifetimes in BTeV. Our main assumption has been that emittance growth and losses due to dynamics stays the same in BTeV as in Run II. Under this assumption, the proton lifetime in BTeV is almost the same as in Run II. Anti-proton lifetimes will approximately double because there is only 1 experiment. There will be a modest increase in the luminosity lifetime from its present value of 8 hrs. The change in luminosity lifetime is small because emittance growth is the largest contributor to the luminosity lifetime and the growth rate is not likely to change much in BTeV.

A Appendix: Error Harmonics

Table A.1 shows the multipole harmonics assumed for the C0 IR magnets. These measurements were taken with the LHC prototype magnets at 215 T/m (11922A). The harmonics are reported in units of 10^{-4} at a reference radius of 17mm. The indexing of the harmonics corresponds to the European convention so that e.g. (b_3, a_3) refer to normal and skew sextupole harmonics. The harmonics are a weighted average over body and the end fields.

Harmonic	Average	Sigma
b3	0.31	0.47
b4	0.02	0.48
b5	-0.03	0.13
b6	-0.02	0.45
b7	-0.01	0.03
b8	0.00	0.02
b9	0.03	0.01
b10	0.00	0.02
a3	-0.57	0.65
a4	0.30	0.39
a5	-0.38	0.18
a6	-0.04	0.11
a7	0.01	0.03
a8	0.01	0.03
a9	-0.02	0.03
a10	-0.03	0.02

Table A.1: Summary of LHC quadrupole harmonics used for the tracking with the C0 IR magnets. Data from obtained from G. Velev in the Technical Division.

The field expansion in terms of these harmonics is

$$B_y + iB_x = 10^{-4} B_{ref} \sum_{n=1} (b_n + ia_n) \left(\frac{x + iy}{R_{ref}} \right)^n \tag{A.1}$$

where B_{ref} is the field at the measured at the reference radius R_{ref}. Within the quadrupoles, $B_{ref} = B' R_{ref}$.

References

[1] Design of an Interaction Region at C0 in the Tevatron, Beams-doc 1001-v5 (September 2004)

[2] T. Sen and M. Syphers,*Second order chromaticity of the Interaction Regions in the Collider*, Proc. 1993 IEEE Part. Acc. Conf, 140 (1993)

[3] K.L.F. Bane et al.,*Phys. Rev. STAB*, **5**, 084403 (2002)

[4] T. Sen, B. Erdelyi, M. Xiao, V. Boocha, *Beam-beam effects at the Fermilab Tevatron: theory*, PRSTAB **7**, 041001 (2004)

[5] T. Sen, M. Xiao, *Beam-beam interactions in Run IIa*, Beams-doc-217-v1 (2002)